Pergamon

Engineering Failure Analysis, Vol. 5, No. 2, pp. 149–169, 1998

Printed in Great Britain
1350–6307/98 $19.00 + 0.00

PII: S1350–6307(98)00013–2

ADVANTAGES OF FLUORIDE ION CLEANING AT SUB-ATMOSPHERIC PRESSURE

WARREN MIGLIETTI* and FRITZ BLUM

Division of Materials Science and Technology, CSIR, PO Box 395, Pretoria, Republic of South Africa

(*Received* 3 *February* 1998)

Abstract—The fluoride ion cleaning (FIC) process is used to assist in the successful braze repair of nickel-based superalloy components. This process is especially effective in removing deeply embedded oxides in wide and narrow cracks typically found in aircraft parts such as in combustors and turbine blades and vanes. Where Al and Ti are present in the base metal, the FIC process depletes these elements from the surface, thereby improving the braze flow and repair of the cracked components. The objective of this paper is to highlight the benefits of using the FIC process at sub-atmospheric pressure. To achieve this, firstly entailed designing and producing specimens suitable to study the fatigue crack behaviour of brazed repaired cracks/joints under mechanical and thermal loading. The cracks/joints prior to brazing were either in an unclean form, i.e. had an oxide layer on, or were fluoride ion cleaned at sub-atmospheric pressure. Fatigue crack propagation tests under constant load as well as under constant stress intensity factor range were conducted in order to study fatigue crack growth characteristics in the parent and braze repaired area. In addition, the resistance to thermal cycling was investigated using single-edge wedge specimens containing brazed repaired joints. Two different braze materials were also under investigation.

For the unclean crack specimens, abnormally high crack growth rates were obtained from the brazed repaired area as compared to parent Ni-based material; whereas for the fluoride ion cleaned crack specimens, lower crack growth rates were experienced. Similarly for the unclean crack specimens, the thermal fatigue crack initiation life was significantly shorter compared with the fluoride ion cleaned crack specimens. © 1998 Published by Elsevier Science. All rights reserved.

Keywords: Fatigue crack growth, gas-turbine failures, joint failures, thermal fatigue.

1. INTRODUCTION

Experience in the gas turbine repair industry has shown that Ni- and Co-based superalloy components containing Al and Ti, especially vanes as seen in Figs 1–3, severely oxidise to form

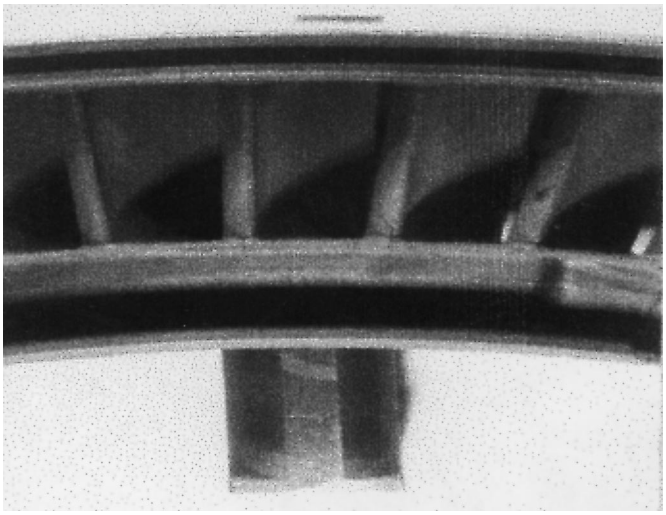

Fig. 1. Severely oxidised narrow, deep cracks on an IN-738 T56, 2nd stage vane.

* Author to whom correspondence should be addressed.

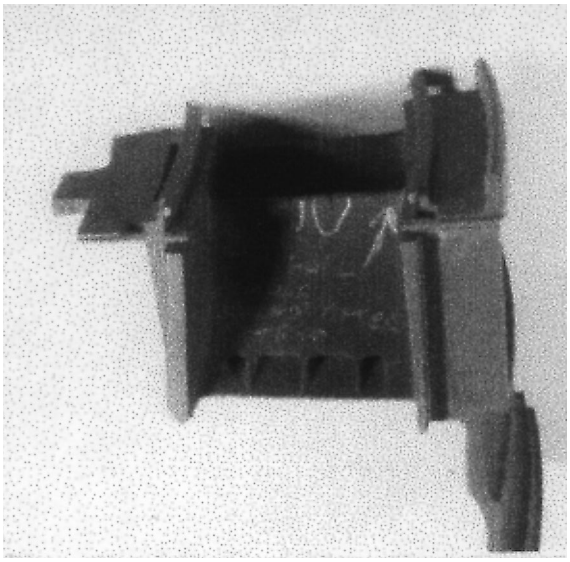

Fig. 2. Severely oxidised wide cracks on an IN-713 T56, 1st stage vane.

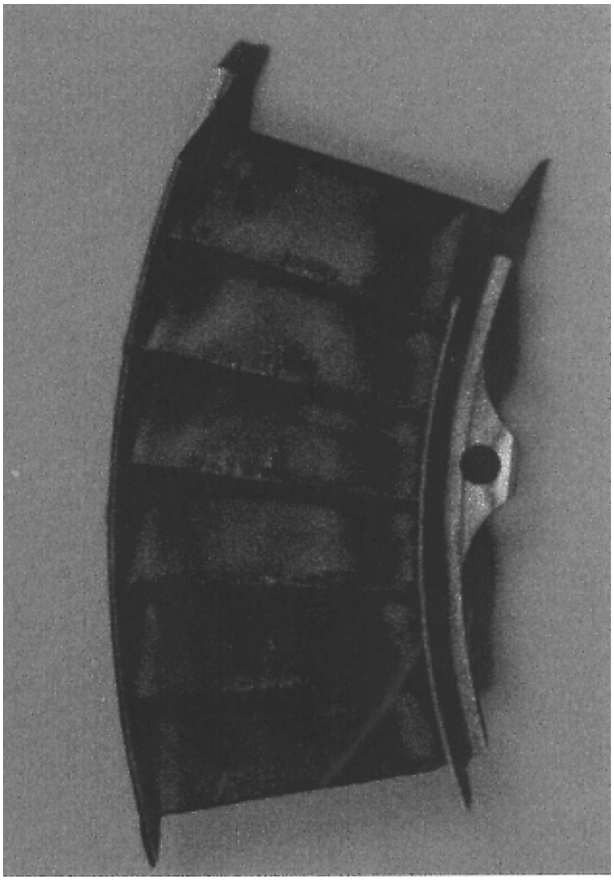

Fig. 3. Severely oxidised cracks on a X-40 Viper, 1st stage vane.

complex spinels on the component surfaces that can penetrate deeply into existing cracks. Currently only cleaning methods using HF gas are capable to removing these deeply embedded oxides. This will allow successful vacuum braze repair to be undertaken.

Traditionally the FIC process was performed at atmospheric pressure (760 torr) but experience

has shown that it only works well when cleaning wide cracks. Therefore, for successful cleaning of narrow deep cracks, the FIC process should be performed at sub-atmospheric pressure. The objective of this paper is to prove that the FIC process should ideally be performed at sub-atmospheric pressure, by conducting fatigue crack propagation (FCP) tests under constant load and under constant stress intensity factor in order to evaluate the crack growth characteristics of FIC and unclean brazed joints in 3 types of single crystal (SC) alloys. In addition, the resistance to thermal cycling was investigated using single edge wedge specimens containing brazed joints.

The HF gas fluoride iron processing equipment is specially designed (by Ti-Coatings Inc.) to use HF gas directly, as opposed to equipment that use precursor compounds such as chrome fluoride (CrF_2) or tetrafluoroethylene (TFE) as the source of HF.

The process subjects the oxidised or sulphidised components to a highly reducing gaseous atmosphere of hydrogen and hydrogen fluoride at high temperatures. The temperature the process is undertaken at, varies from 900°C to 1000°C depending on the Ni-base substrate material being cleaned. (As this is a proprietary process, the actual temperature used in this work will not be documented.)

The HF and H_2 gas is introduced into the system through precision metering, such that the process control parameters of time and gas concentrations can be precisely controlled and tailored for each substrate material. The H_2 and HF cycles can be alternated (pulsed) to ensure complete removal of deeply embedded oxides. The HF concentration varies from 2 to 20%. Similarly as this is a proprietary process, the actual HF concentration used in this work will not be documented.

The gas is directed uniformally over the parts to be processed using an unique gas distribution system. The end products gas, containing H_2 and fluoride reaction products is then scrubbed and neutralised.

The typical chemical reactions that take place in the reactor chamber are:

- $3HF + Al_2O_3$ (on substrate) $- 2AlF_3 + 3/2H_2O$
- $3HF + Al - AlF_3 + 3/2H_2$ (depletes Al from surface)
- $4HF + TiO_2$ (on substrate) $- TiF_4 + 2H_2O$
- $4HF + Ti - TiF_4 + 2H_2$ (depletes Ti from surface)

The typical chemical reactions that take place in the scrubber are:

- $HF + NaOH - NaF$ (soluble) $+ H_2O$ (neutralises HF)
- $H_2 + NaOH - H_2$ (off/spent gas which is discharged to atmosphere)
- $AlF_3 + TiF_4 + NaOH$—soluble fluorides

2. EXPERIMENTAL PROCEDURES

The nozzle guide vanes (composition given in Table 1) shown in Figs 1–3, were fluoride ion cleaned under sub-atmospheric pressure and vacuum brazed, whereas others were cleaned at atmospheric pressure and vacuum brazed. A metallurgical evaluation was undertaken, to compare if the braze wetted the walls of the crack and to determine the depth the braze would flow.

For the fatigue crack propagation (FCP) tests, slots having a width of 0.4–1 mm were cut by wire erosion into compact tension (CT) specimens, normally used to conduct FCP tests. Note, the width of these slots is greater than 0.1 mm; thus conventional narrow gap brazing cannot be utilised, and a wide gap braze technique had to be used. Two braze filler metals were utilised and these are referred to as braze O and braze N. The compositions of these are not documented because they

Table 1. Nominal composition (wt %) of vane materials

Alloy	Ni	Cr	Co	Mo	W	Ta	Cb	Al	Ti	Fe	B	Zr	C
IN-738	61	16	8.5	1.7	2.6	1.7	0.9	3.4	3.4	—	0.010	0.05	0.11
IN-713	74	12.5	—	4.2	—	—	2	6.1	0.8	—	0.012	0.1	0.12
X-40	10	25.5	54	—	7.5	—	—	0.6	—	—	—	—	0.5

are proprietary. The substrate material was either CMSX-4, SMP14 and SMP31. The compositions except for the latter are shown in Table 2 (because SMP31 has not been patented yet). All the alloys are typical 2nd generation single crystal (SC) materials.

The CT samples were oxidised at 800°C in a furnace and then subsequently fluoride ion cleaned or alternatively left in an oxidised condition.

The brazed specimens were then ground and where necessary, the notch was re-sharpened by wire erosion to produce standard FCP test pieces. Figure 4 shows the brazed CT specimen types used in the present work to study fatigue characteristics of brazed CMSX-4, SMP14 and SMP31. In type I, the brazed joint can be seen as an extension of the notch (further referred to as CT1 specimen) as shown in sketch (a) while sketch (b) represents the type 2 specimen with the brazed joint oriented normal to the notch and consequently normal to the crack growth direction (further referred to as CT2 specimen). The distance between the notch tip and the braze was about 12 mm in order to capture FCP data from the parent metal as well.

Two different FCP tests were conducted. Using CT1 specimens, the tests were performed in air under constant load amplitude ΔP cycling at a load ratio of $R = 0.1$ and a frequency of 2 Hz. In contrast, the CT2 specimens were tested under conditions of constant stress intensity factor range ΔK (decreasing load conditions). The ratio of the applied minimum stress to maximum stress was 0.1 and the test frequency was 2 Hz. The initial tests were conducted at ambient temperature in air using a closed-loop servo-hydraulic mechanical testing system. System control and data acquisition

Table 2. Nominal composition (wt %) of SC materials used

Alloy	Cr	Co	Mo	W	Ta	Re	Al	Ti	Hf	Nb	Ni
CMSX-4	6.5	9	6	6	6.5	3	5.6	1	0.1	0	bal
SMP14	4.8	8.1	1	7.6	7.2	3.9	5.4	—	—	1.4	bal

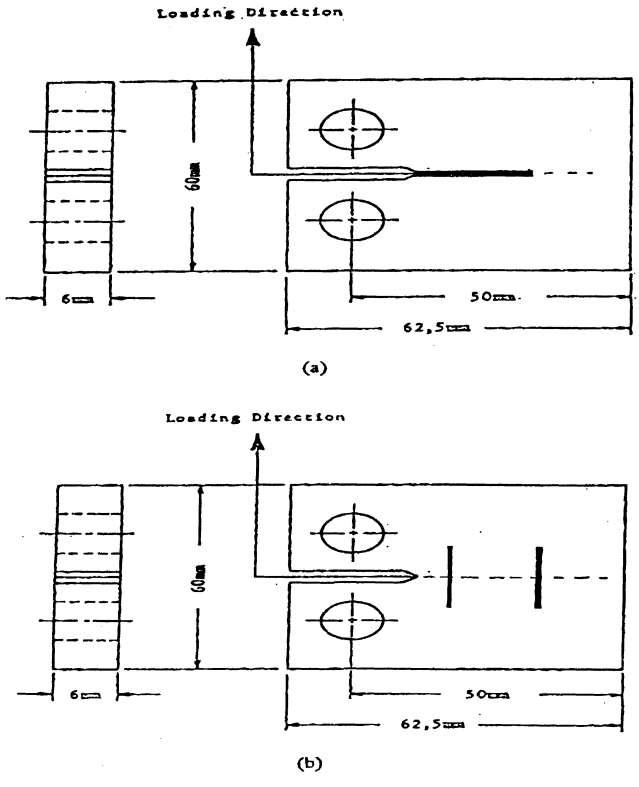

Fig. 4. Specimens used for fatigue crack growth testing of brazed CMSX-4.

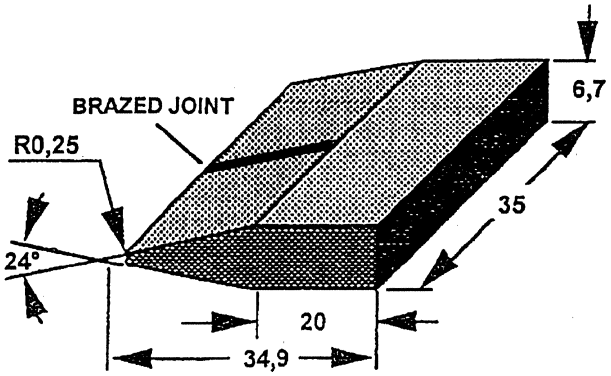

Fig. 5. Brazed SEW specimen used for TF testing.

were executed by an Instron software package in accordance with ASTM E647 standard testing procedures.

The fracture surface of the tested specimens were then studied in a scanning electron microscope (SEM). The fractographic observations were normally made close to the centre section of the specimens and corresponding crack length measurements along the surface were made with the vernier stage of the SEM in order to estimate the corresponding stress intensity factor ranges in the case of constant ΔP testing.

For the thermal fatigue (TF) tests slots having a width and length of 0.5 and 8 mm respectively were machined by wire erosion into flat bars of CMSX-4 having the approximate dimensions of $40 \times 40 \times 7$ mm. These slots were then oxidised, fluoride ion cleaned and then filled by brazing using two different materials, referred to as O-braze and N-braze. Subsequently single-edge wedge (SEW) specimens were then prepared by wire erosion with the brazed joints normal to the thin edge (see Fig. 5). These type of specimens were then used for thermal fatigue (TF) testing using a testing rig at a temperature of 1000°C. The specimens were flame heated and cooled by compressed air. The heating and cooling periods were 180 s and 30 s respectively. The specimens were periodically inspected in the SEM to study the evolution of TF cracking.

3. METALLURGICAL RESULTS AND DISCUSSION

Figure 6 shows the typical oxide layer on a leading edge crack of a T56, 1st stage vane. The greyish oxide layer can clearly be observed in Fig. 7.

Figure 8 shows the oxide layer on a leading edge crack of a 2nd stage, T56 vane after atmospheric FIC. The greyish oxide layer can be clearly seen towards the middle to the bottom of the crack. This shows that for deep cracks (>7 mm) the atmospheric FIC technique utilised does not consistently clean the bottom of the crack completely.

Using a sub-atmospheric FIC cycle and vacuum brazing, a crack on the IN-738 vane results in excellent wetting of the braze to the side walls of the crack, as seen in Fig. 9. The centerline phase is the brittle boride phase that results because the gap was wide, and there was insufficient diffusion time for B to diffuse from the braze joint into the parent metal.

Compared with Fig. 6, there is very little oxide layer present in the cracks of the Viper vane as seen in Fig. 10. This is partially attributed to the low amount of Al + Ti content in the substrate material.

The cracks on the Viper vane were also fluoride ion cleaned under sub-atmospheric conditions and thereafter vacuum brazed. Figure 11(a), (b), (c) and (d) show in all cases the excellent wetting and bonding of the braze to the walls of the crack. Unfortunately, the micrographs also show evidence of brittle boride phases which resulted from inadequate diffusion of the B into the braze.

Figure 12 shows a crack which was brazed repaired, after sub-atmospheric FIC. Although there is porosity in the joint, there is no brittle boride centre line phases and there is once again good wetting and bonding of the braze to the walls of the crack. The crack was only 40 μm wide and thus a long diffusion time was not needed to diffuse the B away from the joint.

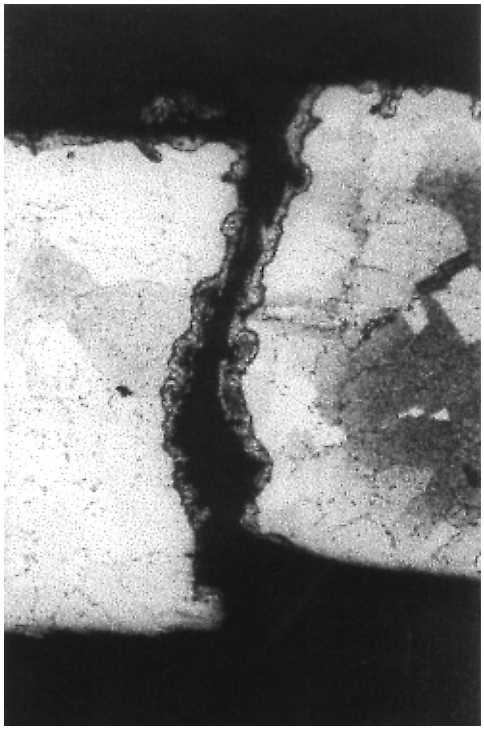

Fig. 6. Oxide layer in the crack of a T56, 1st stage vane, Magnification 100×.

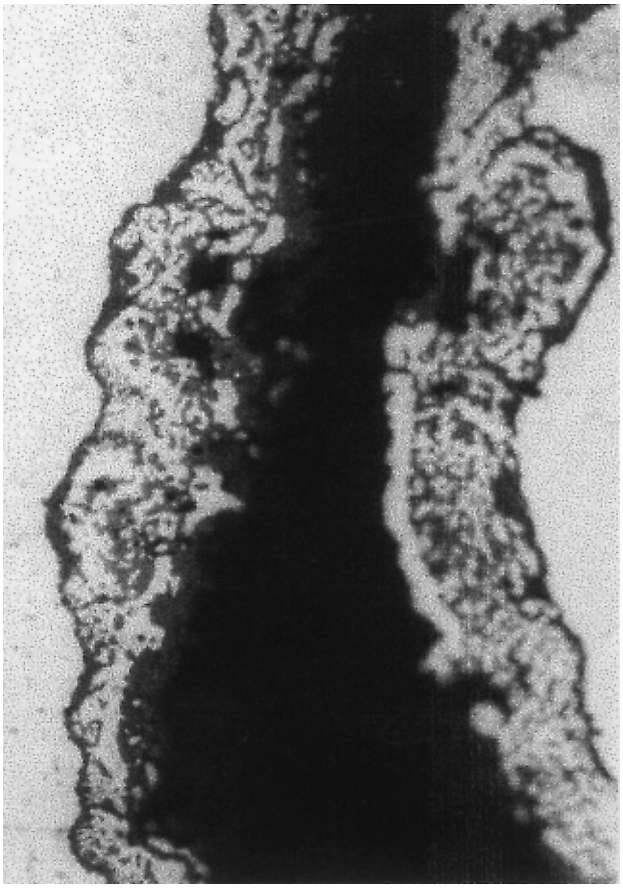

Fig. 7. Greyish oxide layer on side walls of a crack on a T56 vane, Magnification 500×.

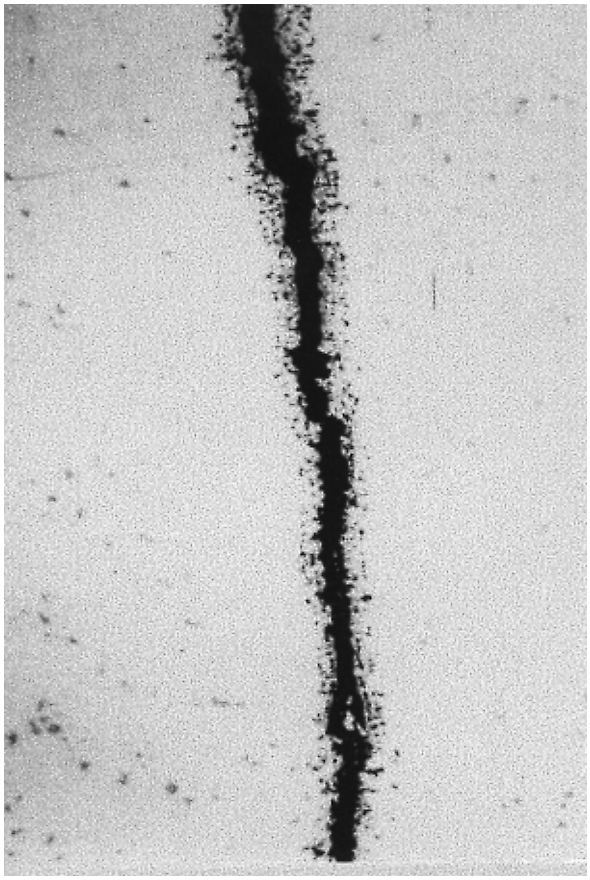

Fig. 8. Oxide layer, still present after atmospheric FIC, on a 2nd stage T56 vane, Magnification 50×.

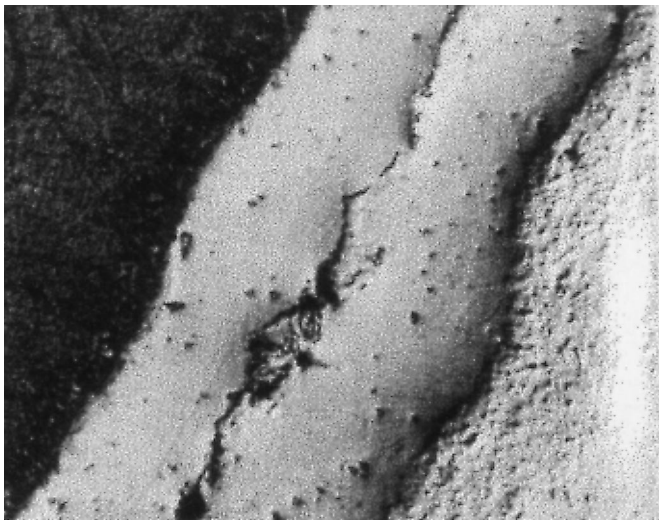

Fig. 9. Sub-atmospheric FIC and vacuum brazing of a crack on a 2nd stage T56 vane, Magnification 500×.

Thus summarising, sub-atmospheric FIC is more suited for removing oxides present in deep, narrow cracks. Successful vacuum braze repairs can therefore be undertaken. There is depletion of Al and Ti from the crack which ranges typically from 5–7 μm. This gives rise to etching effect, in that the braze interface is represented by a dark band on the micrographs as seen in Figs 9, 11(a) and (b) and 12.

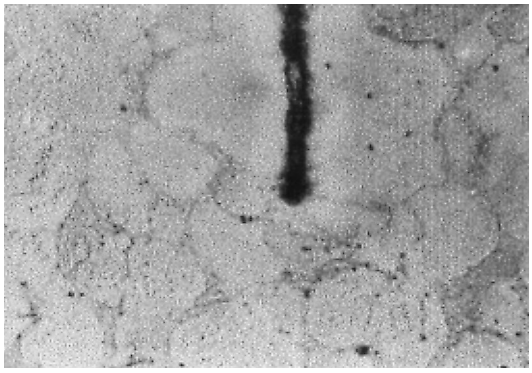

Fig. 10. Little oxide present in the cracks of the Viper vane, Magnification 200×.

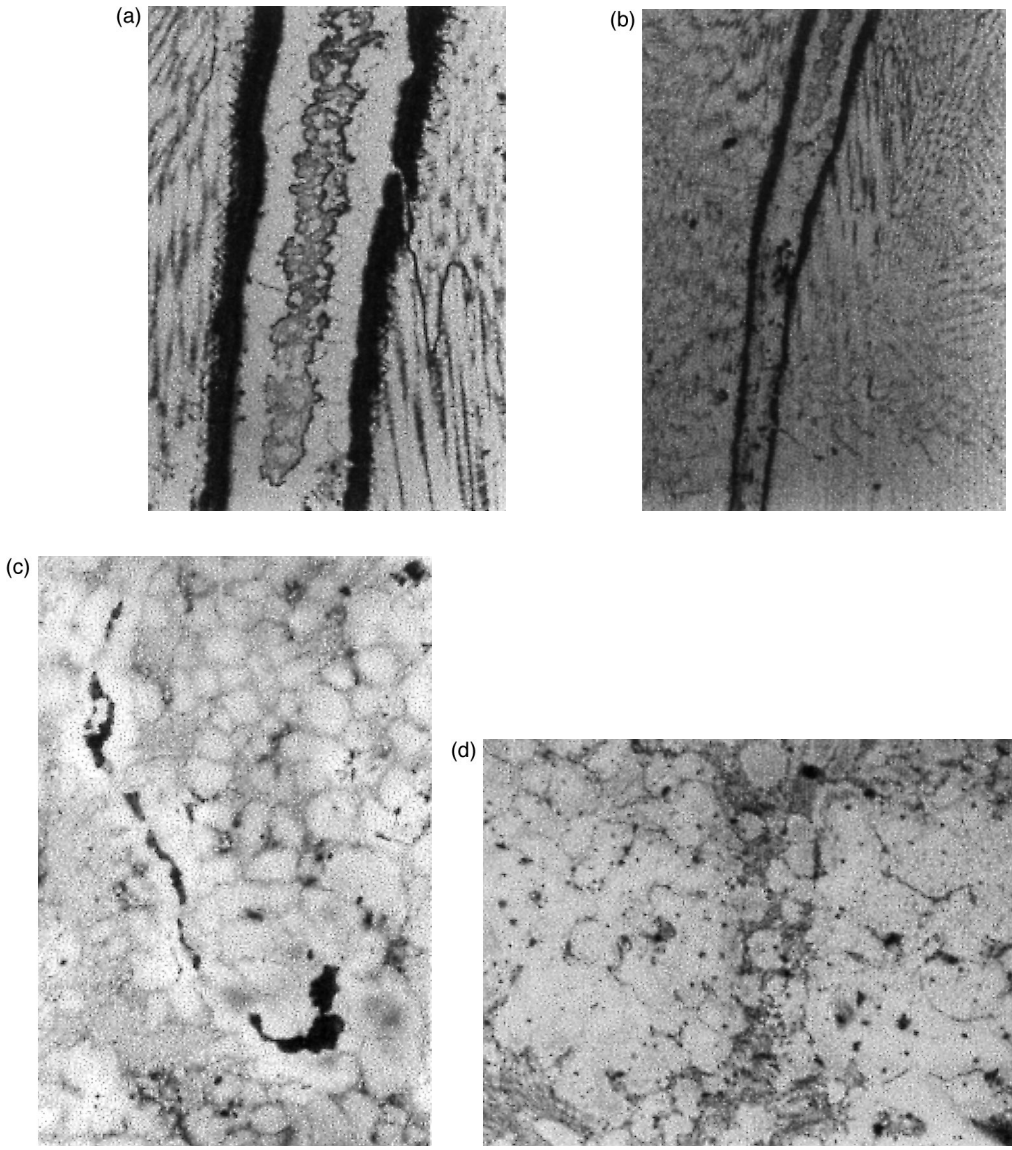

Fig. 11. Various cracks on the Viper vane segment which were fluoride ion cleaned under sub-atmospheric conditions and thereafter vacuum brazed. (a) Magnification 200×; (b) magnification 100×; (c) magnification 100×; (d) magnification 100×.

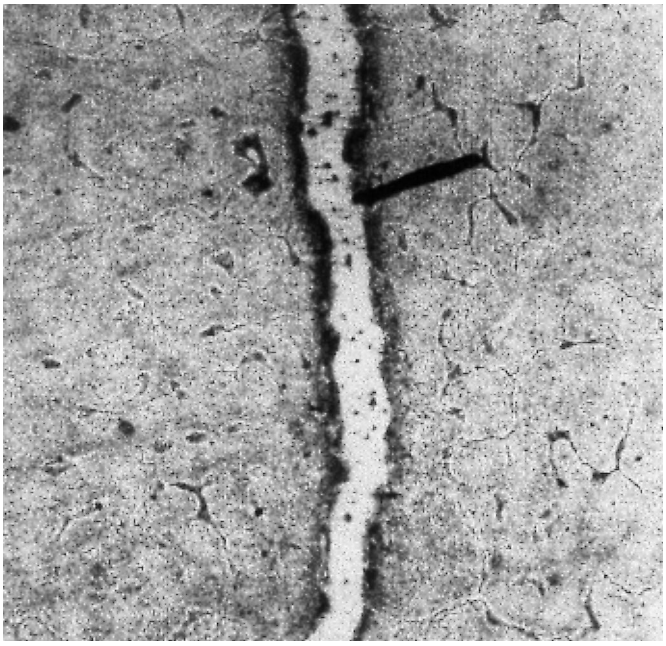

Fig. 12. A crack which was brazed repaired. No centre-line boride phases are present and there is good bonding, Magnification 200 ×.

The use of the sub-atmospheric FIC also results in cracks as fine as 0.010 mm being successfully cleaned.

4. THERMAL FATIGUE RESULTS AND DISCUSSION

For the TF tests, the SEW specimens brazed with the O-braze were not given a fluoride ion cleaning cycle, whereas, the SEW specimens brazed with the N-braze were given a sub-atmospheric fluoride ion clean. As the slots were wire cut, the O-braze had to wet a wire eroded and oxidised surface.

The initial results obtained from brazed SEW specimens subjected to thermal cycling between about 1000°C (total heating time of 180 s) and 200°C (total cooling time of 30 s) are shown in Fig. 13 as a plot of crack length vs number of thermal cycles. The thermally induced fatigue cracks initiated at the edge of each test piece and subsequently growth occurred perpendicular to the edge. It is evident from Fig. 13 that the crack initiation in the O-braze as a result of thermal cycling is

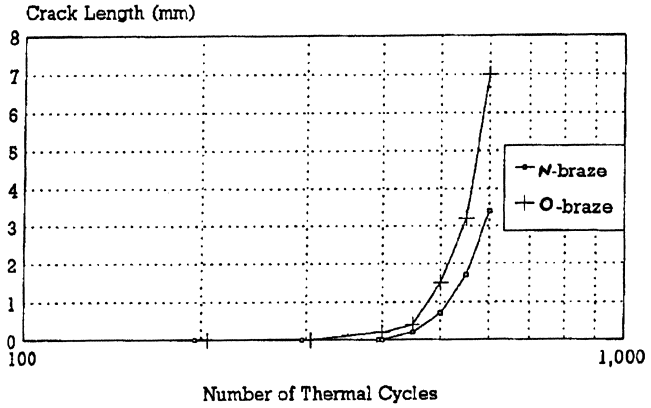

Fig. 13. Thermal fatigue characteristics of two different brazed joints in CMSX-4.

much earlier than in the N-braze. Optical and scanning electron microscope studies show that the initiation and subsequent growth of the TF crack occurred at the braze-parent metal interface for the O-braze. This is not too surprising as this sample was not given a fluoride ion clean cycle and it was expected that there would be a bonding problem, especially at the interface between the braze and the slot. In contrast, cracking was found in the middle of the N-braze. Typical TF cracks close to initiation sites (specimen edge) after 500 thermal cycles are shown in Figs 14 and 15. Figure 16 shows the TF crack propagating at the braze/parent metal interface, whereas Fig. 17 shows the crack through the centre of the braze.

Thus summarising, TF tests were conducted on SEW specimens containing 2 different types of brazed joints, viz one which was fluoride ion cleaned and brazed with the N-braze and the other not fluoride ion cleaned and brazed with the O-braze. The TF crack initiation life defined as the number of thermal cycles to produce a crack of 0.1 mm length, was significantly shorter for the slot/joint not given a fluoride ion clean cycle and brazed with the O-braze compared with the fluoride ion cleaned and brazed with the N-braze. Cracking occurred at the braze-parent metal slot interface for the sample not fluoride ion cleaned, whereas cracking was found in the middle of the braze for the fluoride ion cleaned sample. The cracking was expected to be in the braze because the SC parent metal has good TF properties, whereas the braze would have worst TF life since it contains brittle boride phases and especially for wide gaps as utilised in this study, the braze region at best will only be of an equiaxed structure.

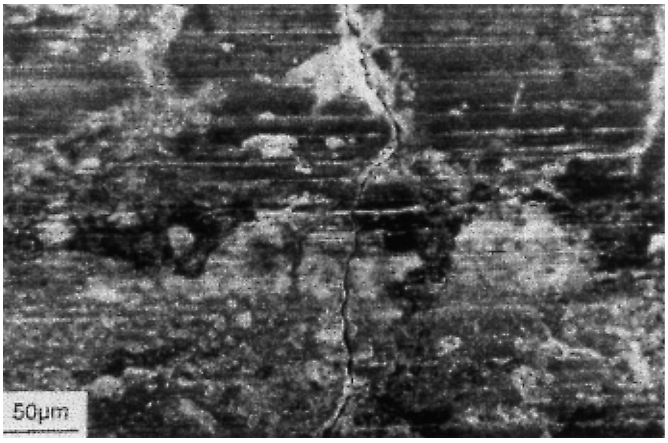

Fig. 14. Thermal fatigue cracking close to initiation site in the N-braze after 500 thermal cycles.

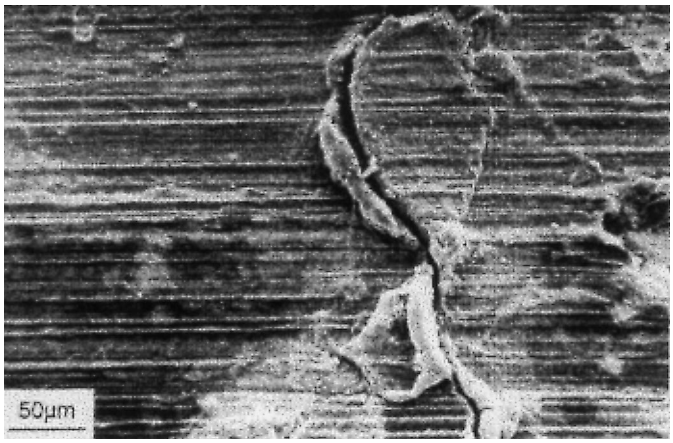

Fig. 15. Thermal fatigue cracking close to initiation site in O-braze after 500 thermal cycles.

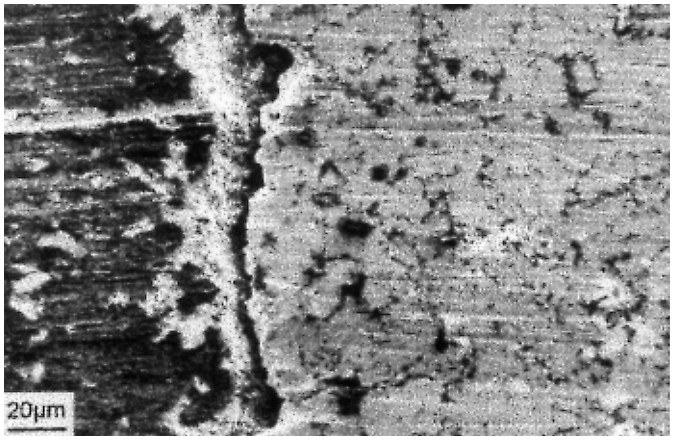

Fig. 16. Scanning electron micrograph showing TF cracking at the parent material/braze material interface.

Fig. 17. Scanning electron micrograph showing TF crack propagation through the middle of the N-braze.

5. CONSTANT ΔK TESTING

The FCP tests under constant ΔK conditions were conducted in order to determine FCP rates and the corresponding fracture surface morphologies in both the O-braze and parent materials i.e., SMP 14, 31 and CMSX-4 at selected constant crack driving forces ΔK. The latter two, viz CMSX-4 and SMP31 specimens were not fluoride ion cleaned prior to brazing. As compared to the CT1 type of specimen, crack growth in the CT2 specimen occurred in the transverse direction of the brazed joint. Figure 18 shows a portion of the plot of crack length vs number of cycles recorded from a CT2 specimen (see Fig. 4) tested at a constant value of $\Delta K = 31$ MPa $\sqrt{\text{m}}$. The crack length in the CMSX-4 parent material increases linearly with number of cycles at a growth rate of about 3×10^{-4} mm/cycle (stage I). This is followed by a drastic change in the cracking behaviour as the crack propagates into the brazed joint (transverse direction) at a growth rate of $\text{d}a/\text{d}N \approx 1.3 \times 10^{-3}$ mm/cycle (stage II). As the crack reached the end of the braze metal it did not propagate into the parent material but changed the direction and crack growth occurred along the braze/parent metal interface, obviously where bonding was very poor. This unexpected behaviour is represented by stage III in Fig. 18, which shows that the crack length remains apparently constant when measured from the loading line of the specimen in the notch direction.

The fractographic studies were focused on the braze material and typical examples of the observed fracture surface morphologies at a constant crack driving force of $\Delta K = 31$ MPa $\sqrt{\text{m}}$ are given in Figs 19 and 20. As expected, the crack growth mechanism in the parent material was crystallographic producing a rather flat fracture surface appearance (part A in Fig. 19). As the crack propagated into the braze material displaying an accelerated crack growth rate, the fracture surface morphology

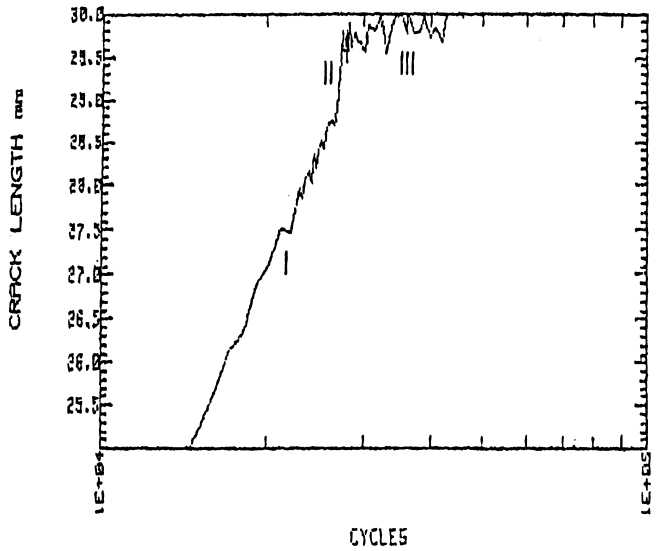

Fig. 18. Plot of crack length vs number of cycles recorded from a brazed CT2 specimen tested at $\Delta K = 31$ MPa $\sqrt{\text{m}}$.

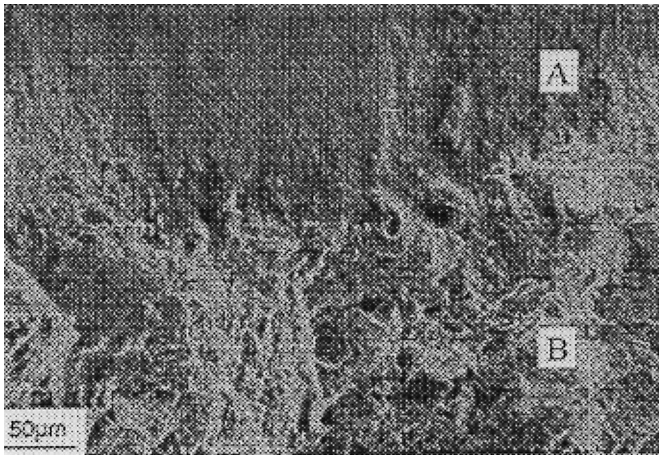

Fig. 19. Fracture morphology of the transition between parent metal (part A) and the brazed joint (part B).

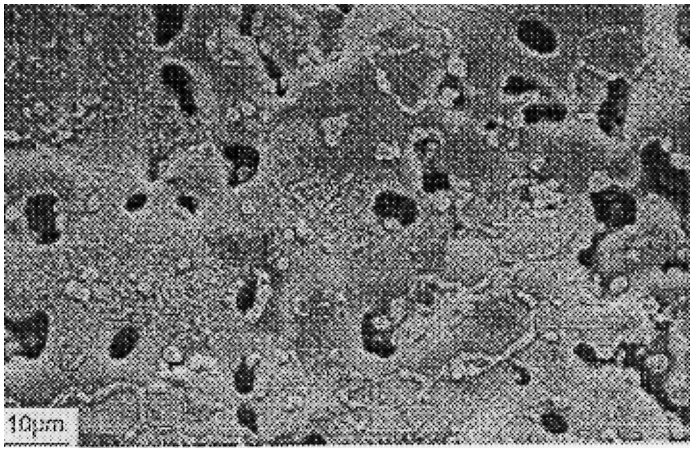

Fig. 20. Fractographic features observed on the surface of the braze material.

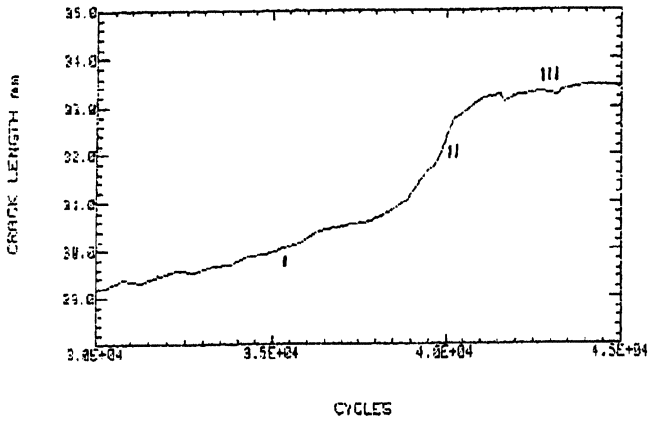

Fig. 21. Plot of crack length vs number of cycles recorded from a brazed CT2 specimen tested at $\Delta K = 30$ MPa $\sqrt{\text{m}}$.

also changed abruptly to a non-crystallographic failure mode (part B in Fig. 19). Unlike the parent material, the fracture appearance of the braze metal was not consistent with a constant ΔK value and the fracture surface consisted frequently of brittle boron-containing phases and inclusions surrounded by ductile tear ridges. Regions of porosity which could be related to unclean surface conditions (because the specimens were not fluoride ion cleaned) can be seen in Fig. 20.

Figure 21 shows a portion of the plot of crack length vs number of cycles recorded from a brazed CT2 specimen of SMP31 which was tested at a constant value of $\Delta K = 30$ MPa $\sqrt{\text{m}}$. The crack length in the parent material shows an approximately linear increase at an average growth rate of about 1.8×10^{-4} mm/cycle. The crack growth behaviour changes dramatically as the crack propagates into the brazed joint showing an average growth rate of about 1.1×10^{-3} mm/cycle.

Typical examples of fractographic studies in the SEM are given in Figs 22–24. As expected, the cracking mechanism in the parent material SMP31 was crystallographic at $\Delta K = 30$ MPa $\sqrt{\text{m}}$ (see Fig. 22). As the crack extended into the braze material resulting in an accelerated FCP rate, the fracture surface morphology also changed dramatically to a rather non-crystallographic failure mode. Figure 23 shows the transition between parent material (part a) and the braze material (part b). It can also be seen from this figure that there is a gap between the braze and the parent material, as a result of inadequate bonding. In contrast to the parent material, the fracture surface appearance of the braze material was not consistent with a constant ΔK value as shown in Fig. 24.

Figure 25 shows a portion of the plot of crack length vs number of cycles recorded from a brazed CT2 specimen of SMP14 which was tested at a constant $\Delta K = 28$ MPa $\sqrt{\text{m}}$. In this case, the CT2 specimen was given a fluoride ion clean cycle prior to brazing. The crack length in the parent metal shows an approximate linear increase at an average growth rate of 0.8×10^{-4} mm/cycle. The crack growth behaviour changed (but not as dramatic as observed with the brazed joints which were not

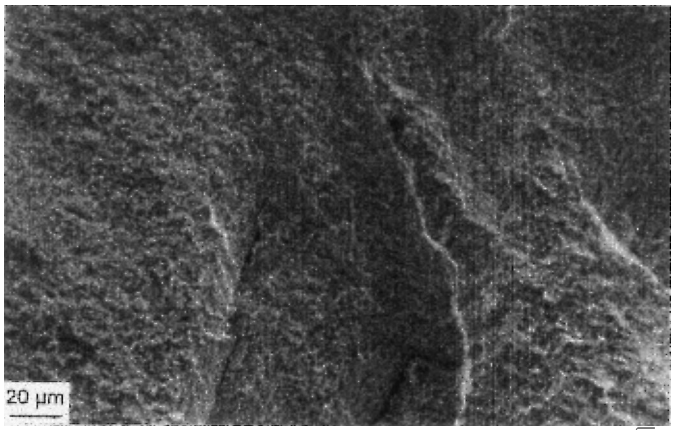

Fig. 22. Fracture surface morphology of SMP31 at $\Delta K = 30$ MPa $\sqrt{\text{m}}$.

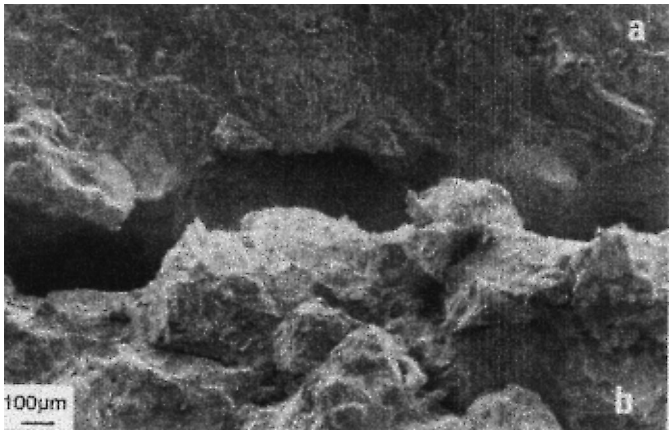

Fig. 23. Fracture surface appearance of the transition region between parent material (part a) and the brazed joint (part b).

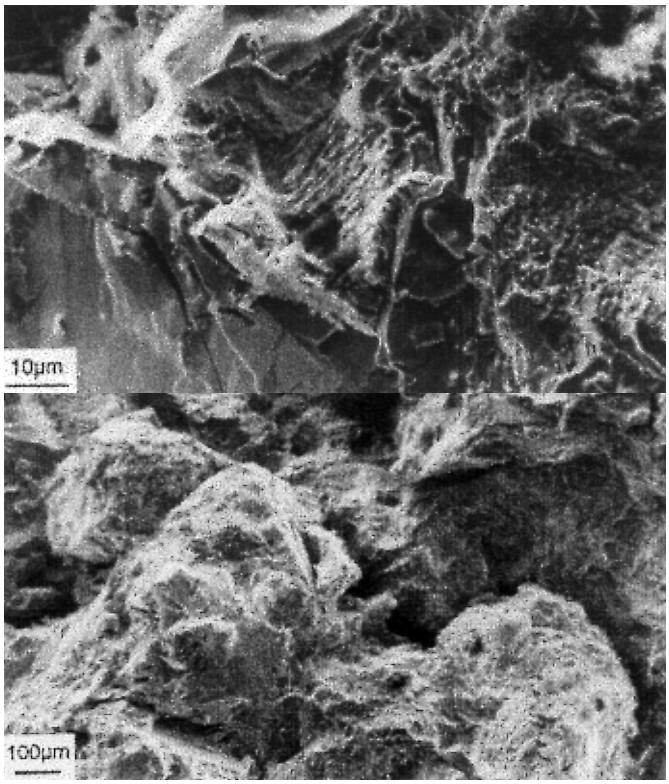

Fig. 24. Different fracture surface morphologies produced in the braze material during FCP testing at a constant value of $\Delta K = 30$ MPa $\sqrt{\text{m}}$.

fluoride ion cleaned (Figs 18 and 21)) as the crack propagates into the brazed joint showing an average growth rate of 3×10^{-4} mm/cycle compared with the previous 1.1×10^{-3} mm/cycle and 1.3×10^{-3} mm/cycle.

6. CONSTANT ΔP TESTING

The variation of FCP rates, da/dN, with the stress intensity factor range, ΔK, is shown in Fig. 26 for a CT1-type specimen which was not fluoride ion cleaned prior to brazing. The experimental data presented in this figure shows a measurable amount of scatter, however, three different 'stages'

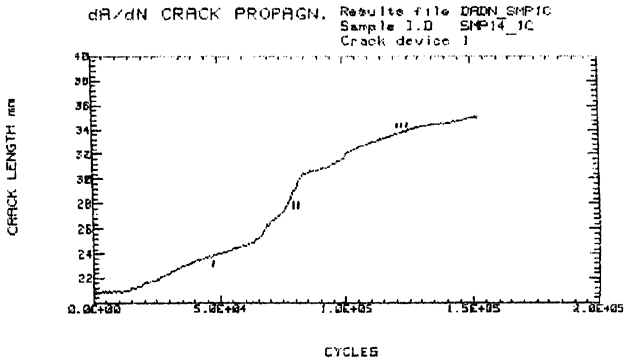

Fig. 25. Plot of crack length vs number of cycles recorded from a fluoride ion cleaned and brazed CT2 specimen tested at $\Delta K = 28$ MPa $\sqrt{\text{m}}$.

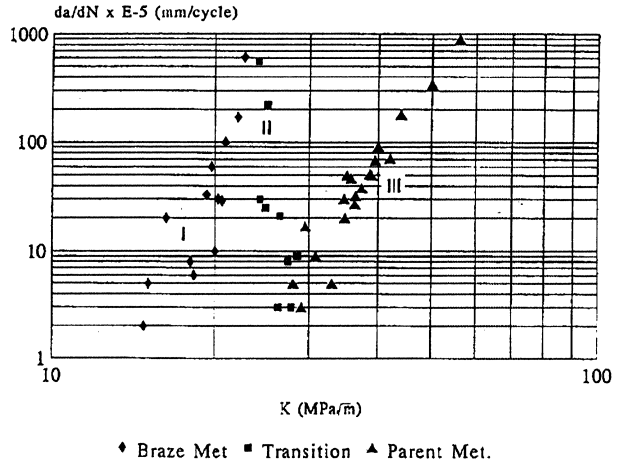

Fig. 26. Fatigue crack growth characteristics of brazed CMSX-4 tested at constant ΔP.

(regions) of crack growth behaviour can be observed. Firstly, stage I represents the characteristics for longitudinal crack growth in the braze metal showing evidence of rapid crack extension. An increase in ΔK from about 20 to 22 MPa $\sqrt{\text{m}}$ increases the FCP rates by more than an order of magnitude. It is also evident that the apparent threshold stress intensity factor range (where crack initiation starts), ΔK_{th}, is only about 14 MPa $\sqrt{\text{m}}$ for the braze material. Secondly, at the end of the brazed joint the FCP rates decrease drastically within the transition zone between braze and parent materials (stage II). Thirdly, stage III shows the FCP characteristics of the parent material CMSX-4. The FCP rates are drastically reduced and the apparent threshold stress intensity factor range ΔK_{th} is significantly higher as compared to the corresponding properties obtained from the braze material. It should, however, be noted that these apparent threshold stress intensity values are higher than the true threshold ΔK_0 values, because the present tests have been conducted under constant ΔP, i.e. increasing ΔK conditions.

The fractographic studies of the fracture surfaces showed that the failure mode in the braze material was not typical of the various stages of fatigue crack growth. At low ΔK values and close to the threshold regime the general failure mode observed is transgranular cleavage producing a rather flat fracture surface appearance. The failure mode changes then systematically with increasing crack length and consequently increasing stress intensity factor range and can at intermediate and high ΔK values normally be described by a non-crystallographic ductility controlled cracking mechanism.

Typical examples of the fracture surface morphology at low and high ΔK values are shown in Figs 27 and 28 for the braze metal. Extensive secondary cracking was observed and the formation of flat transgranular cleavage facets, which are typical of the fatigue crack growth mechanism at low growth rates, appears to be obstructed by the presence of brittle phases within the braze metal

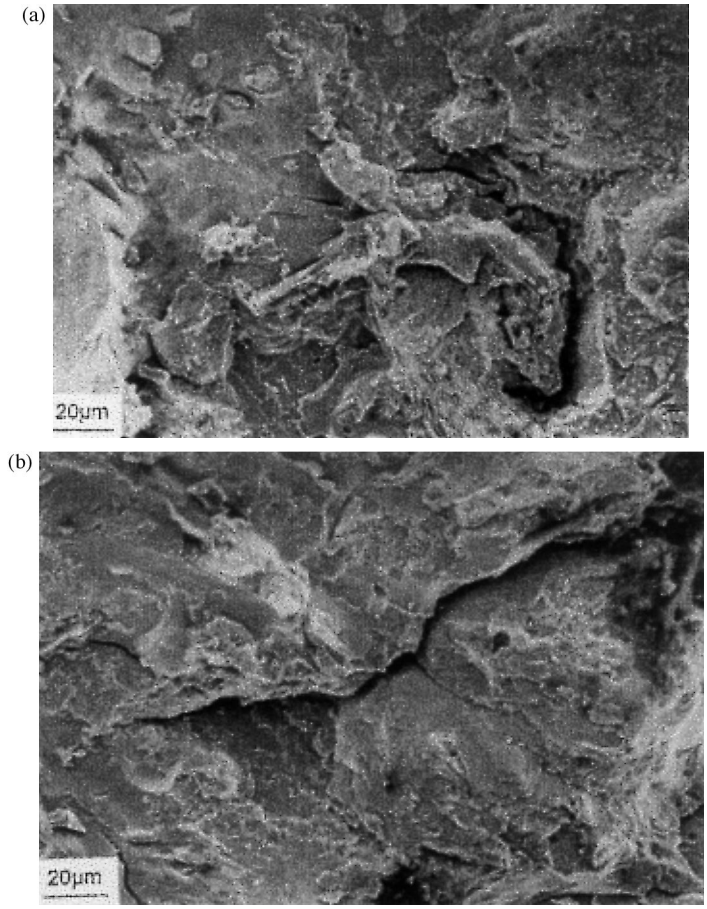

Fig. 27. Scanning electron micrographs of the fracture surface of the braze material at low ΔK value.

(see Fig. 27). No evidence of a crack-tip plasticity controlled striation mechanism, which is typical for the mid-growth regime, was found at higher ΔK values. Secondary cracks and pores as well as areas of brittle fracture morphologies could be observed on the fracture surfaces, as can be seen from Fig. 28. Such fracture surface morphologies suggest that the cracking is mainly controlled by the material's defect structure and not by the amount of crack opening during cyclic loading.

The fracture surface morphology corresponding to the various stages of fatigue crack growth in the parent material were similar of that observed for single crystal superalloys; transgranular cleavage at low ΔK values, ductility-controlled growth at intermediate ΔK values and quasi-static failure modes prior to crack instability.

The results obtained from a FCP test performed on a brazed CT1 type specimen of SMP14 with the brazed joint, not fluoride ion cleaned, are given in Fig. 29. The FCP rate, da/dN, is plotted as a function of the stress intensity factor range, ΔK, on a double-logarithmic scale. Despite the measurable amount of scatter found in the experimental data, three different regions or stages of crack growth can be observed. Stage I represents the crack growth behaviour of the braze material showing rapid crack extension. It is evident from this figure that the apparent threshold stress intensity, ΔK_{th}, is only about 14 MPa $\sqrt{\text{m}}$ for the brazed joint. At the end of the brazed joint, the transition between braze and parent metal (stage II), the FCP rates initially decrease and then increase again as the crack propagates into the parent material. Region III shows the FCP behaviour of the parent material. The apparent threshold stress intensity is significantly higher than that of the braze joint. It should be noted that the apparent threshold behaviour should not be regarded as true threshold behaviour because the present tests were undertaken under constant load (increasing ΔK) conditions. For the determination of the true threshold stress intensity where the growth rates become increasingly small, a decreasing ΔK (load-shedding) technique should be used.

The fractographic studies of the fracture surfaces showed that the failure mode in the braze

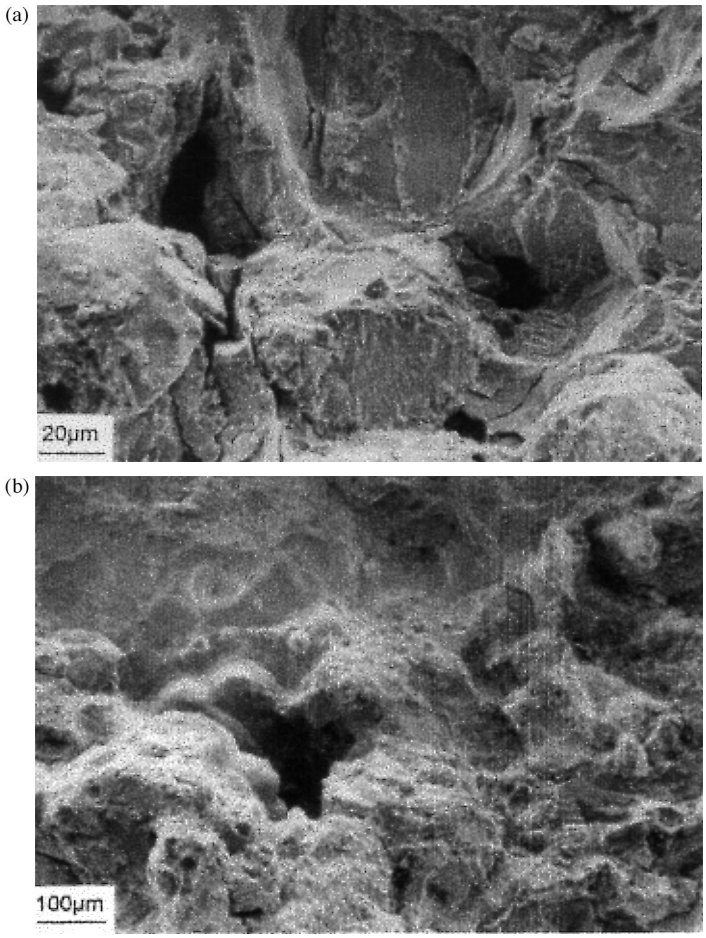

Fig. 28. Scanning electron micrographs of the fracture surface of the braze material at intermediate ΔK value.

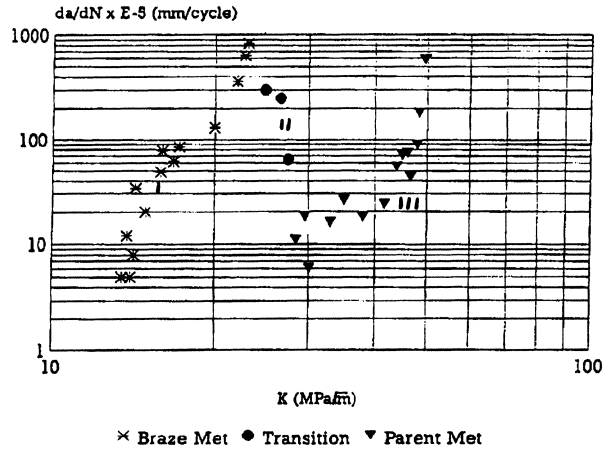

Fig. 29. Plots of FCP rates, da/dN, vs stress intensity factor range, ΔK, for brazed SMP14.

material was not typical of the various stages of fatigue crack growth. At low ΔK values and close to the threshold regime, the general failure mode observed is transgranular cleavage producing a rather flat fracture surface appearance. The failure mode changes then systematically with increasing crack length and consequently increasing stress intensity factor range and can at intermediate and high ΔK values normally be described by a non-crystallographic ductility controlled cracking mechanism.

Typical examples of the fracture surface morphology observed on the braze are given in Figs 30–33. At low ΔK values, transgranular cleavage facets were observed (see Fig. 30) which often showed extensive secondary cracks. At intermediate FCP rates, the mechanism of crack growth was still controlled by cleavage as can be seen from Fig. 31. Only one isolated region was found that showed some evidence of striation which is typical for the mid-growth regime. This is shown in Fig. 32.

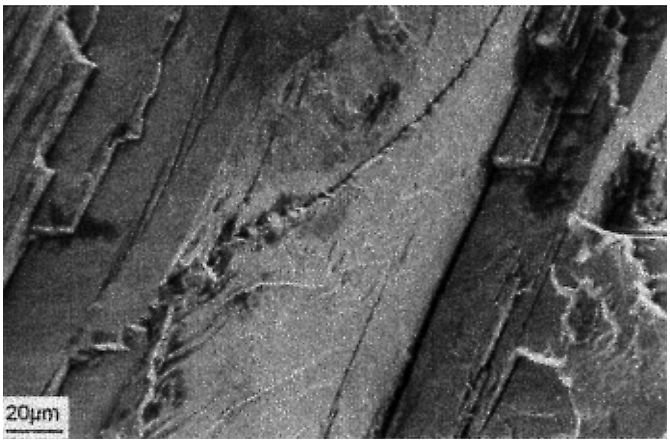

Fig. 30. Scanning electron micrograph of the fracture surface of the braze material at $\Delta K \approx 16$ MPa $\sqrt{\text{m}}$.

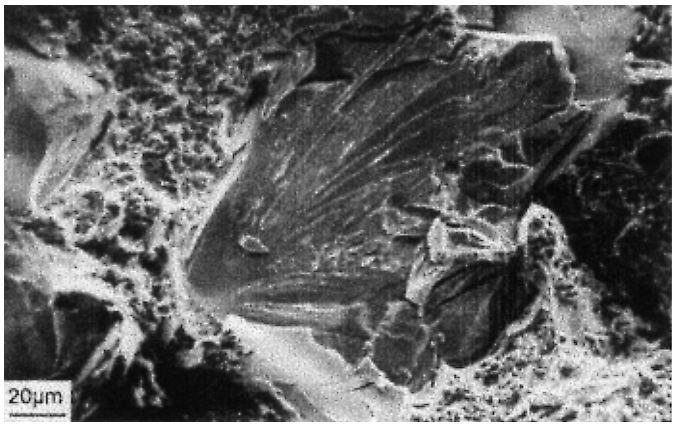

Fig. 31. Typical fracture surface appearance of the braze material in the mid-growth regime.

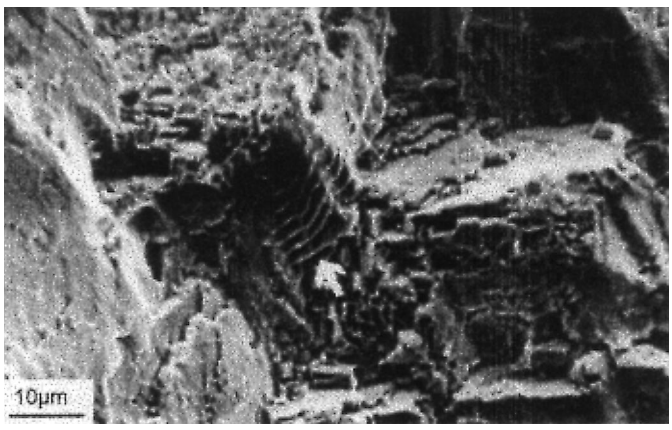

Fig. 32. Isolated striations on the fracture surface of the braze material (see arrow).

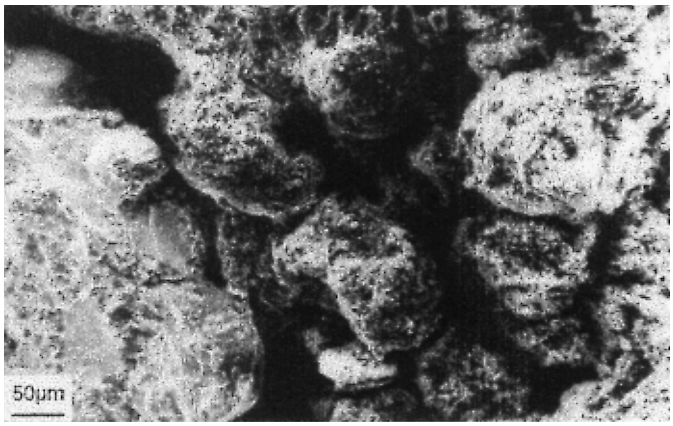

Fig. 33. Scanning electron micrograph showing evidence of inadequate braze processing.

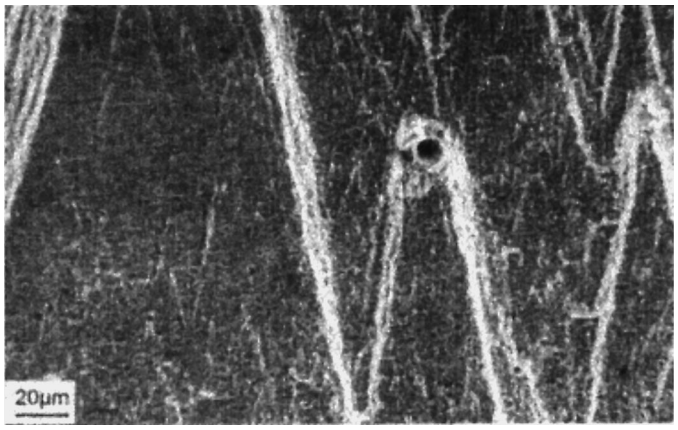

Fig. 34. Scanning electron micrograph of the fracture surface of SMP14 at stage I of crack growth ($\Delta K \approx 20$ MPa $\sqrt{\text{m}}$).

Some areas showed a high density of 'pores' which was probably the result of either inadequate cleaning or incorrect braze processing, as can be seen in Fig. 33.

The fracture surface morphology corresponding to the various stages of fatigue crack growth in the parent material were similar of that observed for single crystal superalloys; crystallographic failure at low ΔK values, ductility-controlled growth at intermediate ΔK values and quasi-static failure modes prior to crack instability. A typical example of stage I crack growth is shown in Fig. 34 for SMP14. Comparable results were obtained for SMP31.

Figure 35 shows a plot of FCP rate, da/dN vs the stress intensity factor ΔK, for a brazed SMP14, CT1 type specimen. In this case the brazed joint was given a fluoride ion clean cycle at sub-atmospheric pressure. Once again the three different stages of FCP behaviour can be clearly identified. Stage I represents the crack growth behaviour of the braze material showing rapid crack growth with increasing ΔK, after exceeding the apparent threshold of ΔK_{th} of 19 MPa $\sqrt{\text{m}}$. As can be seen, the apparent threshold stress intensity ΔK_{th} has increased from 14 MPa $\sqrt{\text{m}}$ to 19 MPa $\sqrt{\text{m}}$ as a result of incorporating the fluoride ion clean cycle prior to brazing.

Details of the fracture surface morphologies can be seen in Fig. 36. The fracture surface of the braze immediately adjacent to the interface exhibited a rather flat appearance similar to that of the parent metal. Such topography is a result of crystallographic crack extension and is typical of FCP at low to intermediate stress intensity factors.

7. OVERALL DISCUSSION

The TF tests showed that the SEW specimens not given a fluoride ion cleaning cycle, had crack initiation much earlier, than the ones given a fluoride ion clean cycle. After 500 thermal cycles, the

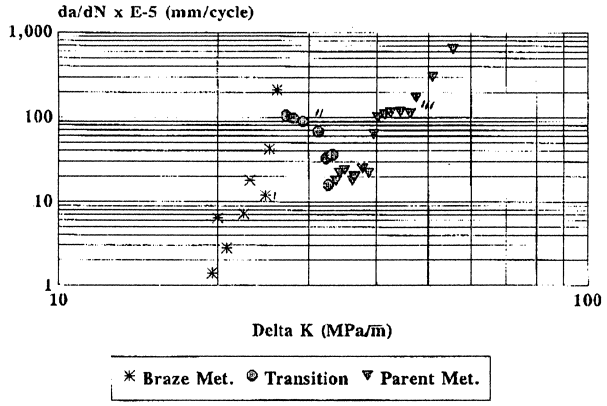

Fig. 35. Fatigue crack growth in brazed SMP14.

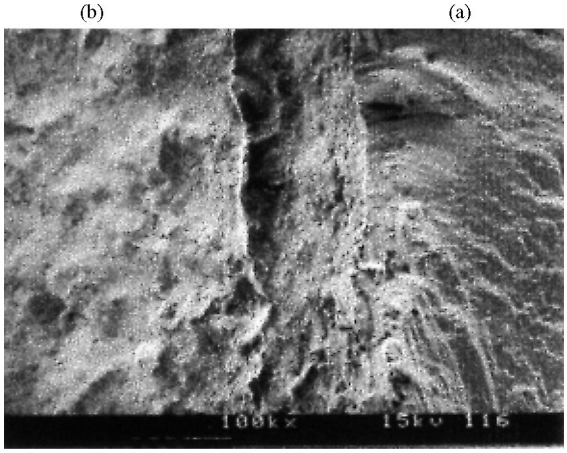

Fig. 36. Fractographic details at the region of good fusion/bonding (a) parent metal and (b) braze metal.

crack length in the samples not fluoride ion cleaned, was 7 mm and fracture occurred at the parent metal/braze interface; whereas, the crack length in the sample fluoride ion cleaned was 3.5 mm and fracture occurred in the middle of the braze. (It is very important to realise that although 2 different braze filler metals were used for the TF tests, the braze cycle used for both was the same and was not fully optimised, because the objective of this paper is not to highlight the values obtained for the brazed joint but to rather highlight the effects of FIC by showing where the fracture path occurred).

The constant ΔK tests showed that the CT2 specimens not given a fluoride ion clean cycle, had a crack growth rate of $da/dn = 1.1 \times 10^{-3}$ mm/cycle at a constant $\Delta K = 30$ MPa $\sqrt{\text{m}}$, whereas the specimens given a fluoride ion clean cycle had a crack growth rate of 3×10^{-4} mm/cycle at a constant $\Delta K = 28$ MPa $\sqrt{\text{m}}$. The crack growth rate of the SC parent metals for CMSX-4, SMP31 and SMP14 was 3×10^{-4} mm/cycle, 1.8×10^{-4} mm/cycle and 0.8×10^{-4} mm/cycle, respectively. (Once again the objective is not to compare the crack propagation rates of the parent metal with that of the brazed joint as the braze cycle was not optimised.) Much of the fracture occurred along the joint interface of the samples not fluoride ion cleaned and this resulted in poor bonding between the braze and parent metal.

The constant ΔP tests showed that the CT1 specimens not given a fluoride ion clean cycle had a threshold stress intensity factor $\Delta K_{\text{th}} = 14$ MPa $\sqrt{\text{m}}$, whereas the specimens given a fluoride ion clean cycle had a $\Delta K_{\text{th}} = 19$ MPa $\sqrt{\text{m}}$.

8. CONCLUSIONS

(1) From the metallurgical evaluation, the use of FIC at atmospheric pressure does not tend to successfully and consistently clean deep cracks, especially greater than 7 mm deep.
(2) The use of FIC under sub-atmospheric conditions allows for successful braze repair on narrow, deep cracks typically found on T56 and Viper vanes.
(3) There is a depletion of Al and Ti from the crack, which ranges typically from 5–7 μm and cracks as fine as 0.010 mm can be successfully cleaned when using FIC under sub-atmospheric pressure.
(4) The TF tests showed that the SEW specimens given a sub-atmospheric FIC cycle, had crack initiation much later than the specimens not given a FIC cycle. After 500 thermal cycles, the crack length in the specimens not given a FIC cycle was 7 mm. The crack length was 3.5 mm for those specimens given a FIC cycle.
(5) The constant ΔP tests showed that the CT1 specimens not given a FIC cycle had a threshold stress intensity factor $\Delta K_{th} = 14$ MPa $\sqrt{\text{m}}$; whereas the specimens given a FIC cycle had a $\Delta K_{th} = 19$ MPa $\sqrt{\text{m}}$.
(6) The constant ΔK tests showed that the CT2 specimens not given a FIC cycle had a crack growth rate of $\text{d}a/\text{d}n = 1.1 \times 10^{-3}$ mm/cycle; whereas the specimens given a FIC cycle had a crack growth rate of 3×10^{-4} mm/cycle.